Article

Growth and Characterisation of Antiferromagnetic Ni₂MnAl Heusler Alloy Films

Teodor Huminiuc [1], Oliver Whear [1], Andrew J. Vick [1], David C. Lloyd [2], Gonzalo Vallejo-Fernandez [1], Kevin O'Grady [1] and Atsufumi Hirohata [2,*]

[1] Department of Physics, University of York, Heslington, York YO10 5DD, UK; teodor.huminiuc@gmail.com (T.H.); owhear@gmail.com (O.W.); andrew.vick@stfc.ac.uk (A.J.V.); gonzalo.vallejofernandez@york.ac.uk (G.V.-F.); kevin.ogrady@york.ac.uk (K.O.)

[2] Department of Electronic Engineering, University of York, Heslington, York YO10 5DD, UK; david.lloyd@york.ac.uk

* Correspondence: atsufumi.hirohata@york.ac.uk

Abstract: Recent rapid advancement in antiferromagnetic spintronics paves a new path for efficient computing with THz operation. To date, major studies have been performed with conventional metallic, e.g., Ir-Mn and Pt-Mn, and semiconducting, e.g., CuMnAs, antiferromagnets, which may suffer from their elemental criticality and high resistivity. In order to resolve these obstacles, new antiferromagnetic films are under intense development for device operation above room temperature. Here, we report the structural and magnetic properties of an antiferromagnetic Ni₂MnAl Heusler alloy with and without Fe and Co doping in thin film form, which has significant potential for device applications.

Keywords: antiferromagnets; Heusler alloys; exchange bias; blocking temperature; spintronic devices

1. Introduction

Antiferromagnetic spintronics has been attracting a lot of attention due to its potential for THz operation and low power consumption [1]. Currently, antiferromagnetic metals, e.g., IrMn₃ and PtMn₃, and semiconductors, e.g., CuMnAs, have been commonly used [2]. However, these materials are fragile against local compositional changes and may not be suitable for miniaturisation. For further investigation towards device applications, it is critical to develop new antiferromagnetic materials, which are robust against nanofabrication, such as oxidation, atomic mixing, edge roughness and post-annealing.

Antiferromagnetic Heusler alloys are good candidates for applications with precise controllability by potential atomic substitutions. In particular, ternary Heusler alloys, e.g., Pt₂MnGa [3], Ni₂MnAl [4,5] and Mn₂VSi [6], have been reported to exhibit antiferromagnetism as schematically shown in Figure 1. Among them, Ni₂MnAl has been studied and has a lattice constant of 0.5812 nm [5], similar to commonly used seed layers and substrates. However, the Néel temperature has been reported to be between 40 °C [7] and 80 °C [4], which will need to be increased for device applications via atomic substitution as previously reported, e.g., for compensated Mn₂.₄Pt₀.₆Ga ferrimagnet [8]. These studies have been based on epitaxial Ni₂MnAl films [9,10] and bulk samples, but not on polycrystalline films with their suitability for devices, e.g., magnetic sensors and recording. Recent reduction in a device size can utilise a single grain in a polycrystalline film to avoid any electrical and/or magnetic scattering at a grain boundary and/or magnetic domain wall.

In this paper, we report on the optimised growth and annealing conditions for polycrystalline Ni₂MnAl films sputtered at room temperature (RT). The optimisation involves (i) post-annealing between ~400 and 500 °C for up to 2 h and (ii) atomic substitution for crystallisation. Point (ii) is highly significant for the tuning of structural and magnetic properties, such as the Néel temperature, blocking temperature and the lattice constant.
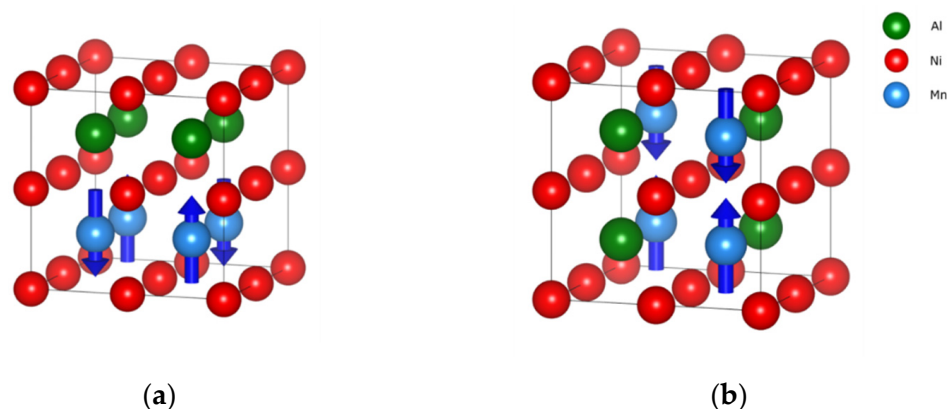
Figure 1. Schematic crystal and spin structures of the pseudo-*B*2-(**a**) I and (**b**)-II phases for Ni$_2$MnAl. Red, blue and green atoms represent Ni, Mn and Al, respectively.

2. Experimental Procedures

100 nm thick Heusler alloy films capped with 2~5 nm of Ru or Ta were deposited onto Si substrates using RF generated remote plasma sputtering. The layers were deposited using a PlasmaQuest high target utilisation sputtering system (HiTUS) with a base pressure of 3×10^{-5} Pa. The plasma was generated by an RF field of 13.56 MHz in an Ar atmosphere of 3×10^{-1} Pa and steered onto the target with a DC bias (V_T) ranging from -250 to -990 V. V_T controlled the deposition rate and the resulting atomic mixing. The typical deposition rate from the stoichiometric Ni$_2$MnAl target using a bias voltage of 990 V was 0.06 nm/s. The growth rate also controls the grain size. Ni$_2$MnAl (25)/CoFe (10) and Co$_2$FeSi (10) (thickness in nm) bilayers were also grown using HiTUS in a similar manner.

The composition of the films was analysed using inductively coupled plasma optical emission spectroscopy (ICP-OES) by InterTek Ltd., confirming near stoichiometry (with some Al deficiency), Ni:Mn:Al = 54.1:28.9:17.0 and 56.1:29.6:14.3 for $V_T = -900$ and -300 V, respectively. The crystalline structures were characterised using out-of-plane (OP) and grazing incidence in-plane (IP) X-ray diffraction (XRD, Rigaku SmartLab) with a Cu $K\alpha$ source and a Ge(220) 2-bounce monochromator. The Heusler-alloy films were annealed in an Ar gas flow (2 L/min.) between 235 and 700 °C for up to 9 h. After each annealing step magnetisation curves were measured using an alternating gradient force magnetometer (AGFM, Princeton Measurements Model 2900) at RT.

3. Results and Discussion

3.1. Ni$_2$MnAl Films

From XRD measurements, a Ni$_2$MnAl(220) principal peak was found once samples were annealed at 700 °C as shown in Figure 2. A well-defined (220) peak was developed OP within the first 90 min of annealing. However, after a further one hour of annealing, no further OP crystalline growth was observed as shown in Figure 2b. As similar to Fe$_{2+x}$V$_y$Al [11], longer annealing induces phase segregation in the Ni$_2$MnAl films as confirmed by the appearance of a ferromagnetic phase. The OP lattice constant of Ni$_2$MnAl was measured to be (0.575 ± 0.001) nm. This is about 1% lower than the theoretically predicted value of 0.5812 nm [5]. There was a transition in the IP (220) peak when the sample was annealed for more than 1.5 h, corresponding to a 1% change in the IP lattice constant from (0.577 ± 0.001) nm to (0.571 ± 0.001) nm, which almost agree with the OP results. The lattice constants of the sputtered polycrystalline Ni$_2$MnAl films are almost 2% lower than the theoretical value, which may be due to the lower crystallinity and the formation of the segregated phases in the films. This is supported by the absence of additional superlattice (200) or (111) peaks in the XRD patterns. Magnetic measurements confirmed that these films show no magnetic response, indicating that they are in an either antiferromagnetic, paramagnetic or compensated ferrimagnetic state.
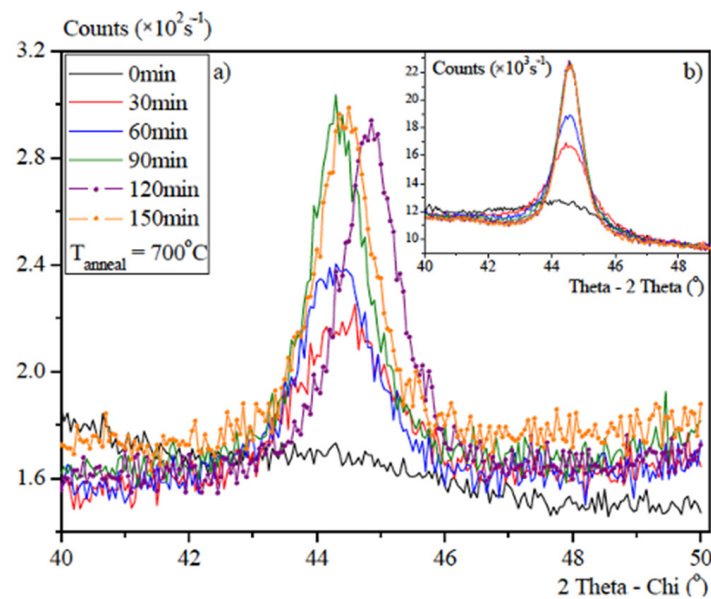
Figure 2. Representative XRD patterns of the Ni$_2$MnAl(220) peaks measured by (**a**) IP and (**b**) OP configurations.

In order to quantify the crystallinity of the Ni$_2$MnAl films measured by XRD, we used a Q factor defined as

$$\text{Q factor} = \frac{\text{Intensity (cps/}^{\circ}\text{)}}{\text{Full width half maximum (FWHM)}} \tag{1}$$

The (220) peaks were used to quantify the *A*2 crystalline ordering (atomic mixing between Ni, Mn and Al), i.e., the increase in Q factor represents the increase in *A*2 ordering, which typically leads to *B*2 ordering (atomic mixing between Ni and Mn) with a coexisting (200) peak and *L*2$_1$ perfect ordering with coexisting (200) and (111) peaks [12].

Given the requirements for device fabrication, annealing temperatures above 500 °C are impractical. Therefore, our optimisation criteria were as follows: (i) we identified the post-annealing condition below 500 °C to maximise the Q factor. The increase in the *A*2 ordering leads to the formation of the pseudo-*B*2 phase, which is theoretically [5] and experimentally [10] predicted to exhibit antiferromagnetism; (ii) we have substituted some constituent elements to investigate the effect on the crystallisation temperature.

The Ni$_2$MnAl samples were post-annealed for up to 6 h at temperatures in the range 250 to 700 °C. There was no *L*2$_1$ crystallisation observed in any of the samples post-annealed at a temperature below 700 °C (see Figure 3). The presence of a small number of *A*2 ordered nanocrystals was indicated in all the as-deposited samples by a weak (220) Ni$_2$MnAl alloy peak at 44.0° with a FWHM of 0.7°. Rocking curves were used to measure the texture of the (220) peak, indicating that the as-deposited grains were aligned within ±15° from the sample surface only for the epitaxial films as reported previously [10]. In a similar Heusler alloy of Fe$_{2+x}$V$_y$Al films [11], a *B*2 phase has been formed when the Q-factor increases over one order of magnitude as compared with the initial *A*2 crystallisation occurred. In this study we applied this criterion to identify the phase transformation in Figure 3.

The corresponding exchange bias are shown in Figure 4 for the Ni$_2$MnAl (25)/CoFe (10) and Co$_2$FeSi (10) (thickness in nm) bilayers post-annealed at 250 and 400 °C for 2 h, which were in the *A*2 and *B*32a phase, respectively, as shown in Figure 3. These magnetisation curves were measured after field cooling to 100 K under an in-plane magnetic field of 20 kOe. No clear exchange bias effect can be seen within the measured temperature range in Figure 4. However, an increase in the coercivity was observed only for the sample annealed at 400 °C forming the *B*32a phase. This may be indicative of coupling between layers, suggesting the Ni$_2$MnAl layer is antiferromagnetic but the corresponding Néel (and

blocking) temperature is below 100 K possibly due to the coexisting disordered phases. Further increase in the annealing temperature leads to the higher crystallinity of Ni_2MnAl as shown in Figure 3 but it induces interfacial mixing in the bilayers causing reduction in the saturation magnetisation. By maintaining the sharp interface between Ni_2MnAl and the neighbouring ferromagnetic layer, an exchange bias can be measured at 100 K or above [10].
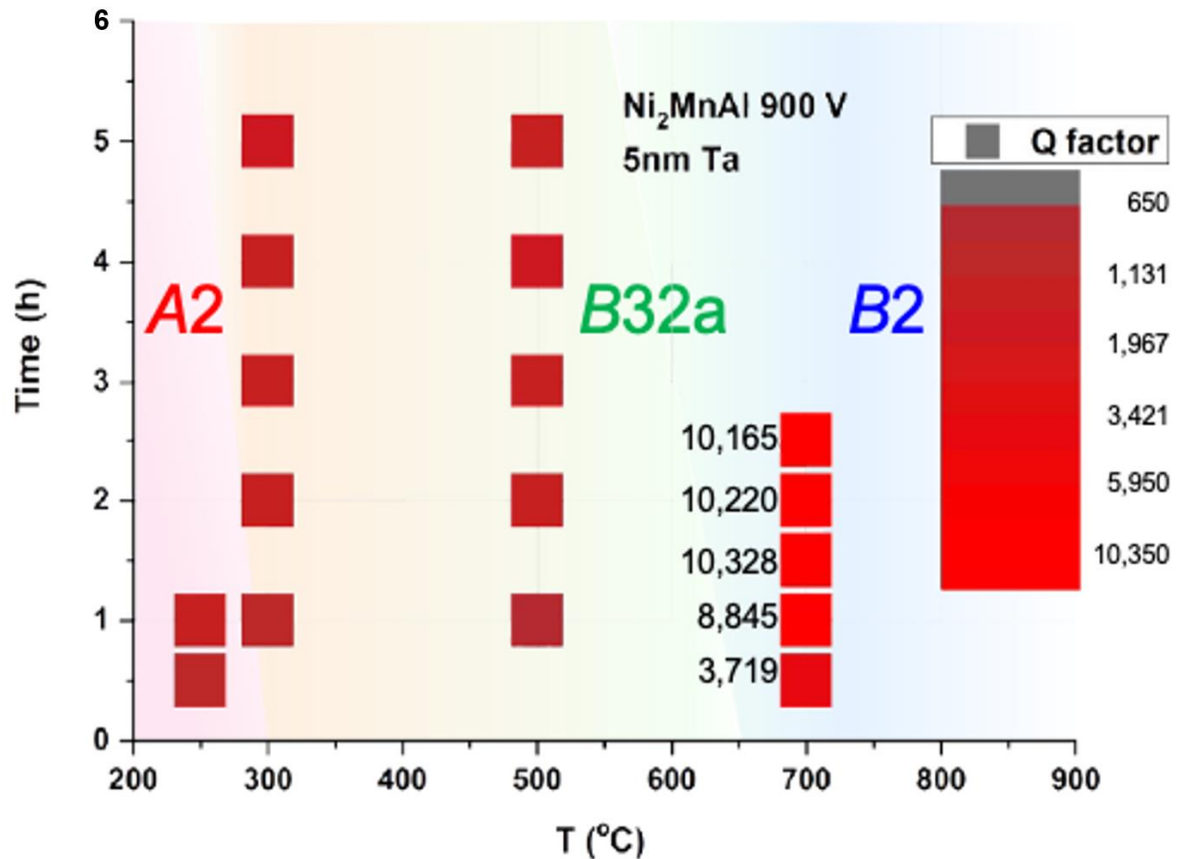

Figure 3. Crystallisation of the Ni_2MnAl thin films indicated by Q factors, including annealing conditions which did not lead to crystallisation. The letters shown next to colour scales indicate the corresponding Q-factors.
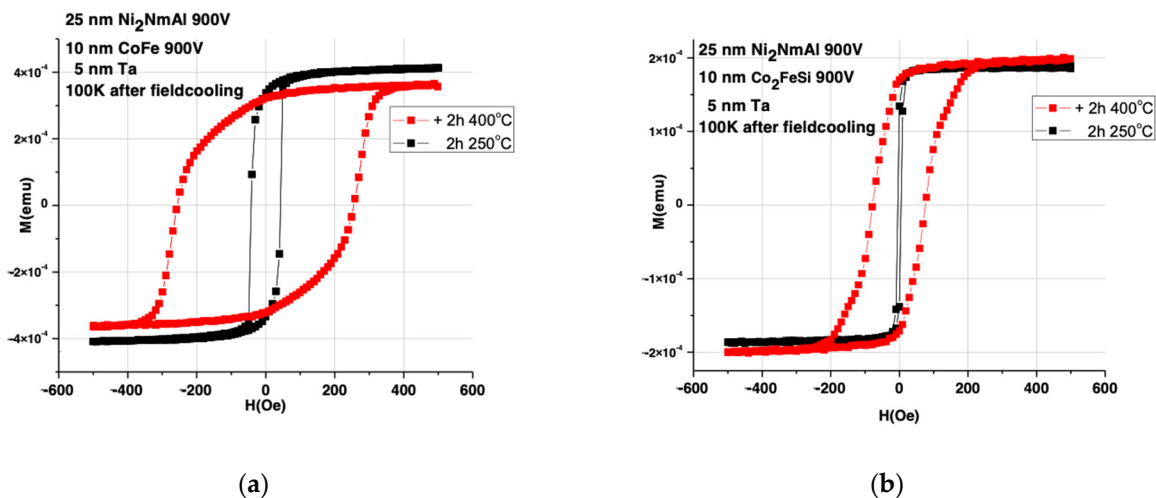

(**a**)   (**b**)

Figure 4. Magnetisation curves of the Ni_2MnAl (25)/(**a**) CoFe (10) and (**b**) Co_2FeSi (10)/Ta (5) (thickness in nm) bilayer post-annealed at 250 and 400 °C for 2 h under the field applications in the plane.

3.2. Ni₂MnAl Films with Atomic Substitutions by Al

As the sputtered Ni_2MnAl films are ~10% Al deficient, one 6 mm diameter Al peg was added to a pre-drilled hole in the sputtering target, achieving Ni:Mn:Al = 49:27:24. With a target utilisation of over 90%, this technique allows for the variation of the film composition in the HiTUS. Figure 5 shows the Q factors for the Al-doped Ni_2MnAl post-annealed at 500 °C, which was found to be the maximum annealing temperature to avoid Al segregation. Similar to the films without Al doping, Ni_2MnAl crystallises at a relatively high temperature. The Al-doped Ni_2MnAl films have therefore the optimum A2 crystal structure after 2~4 h of annealing at 500 °C. The corresponding lattice constants were found to decrease from 0.585 to 0.575 nm after 1 and 4 h of annealing, respectively. This confirms that the lattice constants are similar to those without Al doping except for the sample annealed for 1 h. This agrees with the increase in the Q factors shown in Figure 5, indicating the effect of the Al doping on the optimised crystallisation temperature and crystallinity of Ni_2MnAl is negligible.
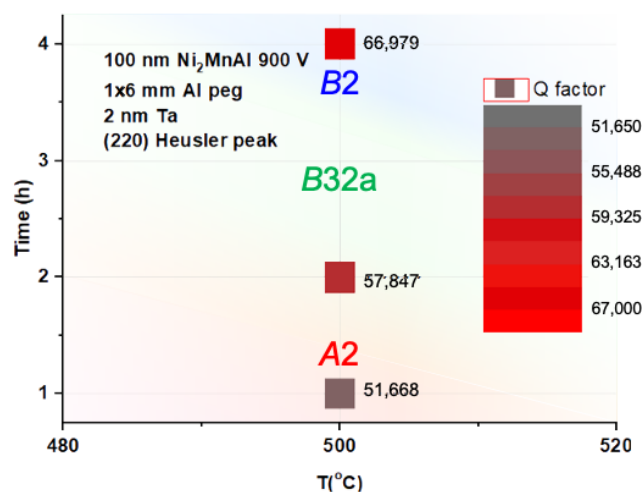

Figure 5. Crystallisation of the ordered Ni_2MnAl thin films doped with a 6 mm Al peg indicated by Q factors.

3.3. Ni₂MnAl Films with Atomic Substitutions by Fe

In order to decrease the Ni_2MnAl crystallisation temperature, an attempt to substitute Ni in the lattice by Fe was made because its covalent radius is greater than that of Ni. This results in the lattice being strained and this may decrease the manganese–manganese nearest neighbour distance to induce antiferromagnetic coupling. However, no crystallisation was found. $Fe_{2+x}V_yAl$ has been studied previously [11], showing that the ordering temperature is lower than that of the Ni_2MnAl thin films. Therefore, it is predicted that doping with Fe can lower the ordering temperature and induce antiferromagnetic ordering in the Ni_2MnAl thin films.

The Ni_2MnAl sputtering targets were doped with two or four Fe pegs with a diameter of 2 mm, effectively making a $Ni_{2-x}Fe_xMnAl$ target. The sputtered Ni_2MnAl films doped with Fe were found to exhibit ferromagnetic behaviour even in the as-deposited state. Almost negligible magnetic moments of (1.5 ± 0.1) µemu, approximately 3×10^{-2} emu/cm³, was measured for the samples grown from the Ni_2MnAl sputtering target doped with two Fe pegs and (2.7 ± 0.1) µemu with four Fe pegs. This small moment was probably induced by Fe segregation. The films were then post-annealed for up to three hours at temperatures between 400 and 500 °C. However, no crystallisation of the Ni_2MnAl Heusler alloy was detected but the average saturation magnetisation increased to (2.0 ± 0.1) µemu and (3.4 ± 0.1) µemu after annealing at 500 °C for 3 h for the films doped with two and four Fe pegs, respectively. This suggests that the Fe segregation is promoted by post-annealing.

3.4. Ni$_2$MnAl Films with Atomic Substitutions by Co

Co-doping was also tested because its covalent radius is greater than that of Ni but is smaller than that of Fe. This may also decrease the manganese–manganese nearest neighbour distance to induce antiferromagnetic coupling as predicted for the case of the Fe doping. The corresponding lattice constants for one Co peg were found to decrease from 0.584 to 0.580 nm after 1 and 5 h of annealing, respectively. Co$_2$MnAl has hence been reported to have an ordering temperature lower than Ni$_2$MnAl [13,14], suggesting that the Co doping may also lower the ordering temperature and promote antiferromagnetic ordering.

The Ni$_{2-x}$Co$_x$MnAl sputtering targets were used adding one or two Co pegs with a diameter of 6 mm onto the Ni$_2$MnAl target, achieving Ni:Co:Mn:Al = 56:9:20:15 and 51:15:20:14 for one and two Co pegs, respectively. The sputtered films exhibited paramagnetic behaviour in the as-deposited state. The films successfully crystallised after post-annealing at temperatures between 400 and 500 °C for two hours as shown in Figure 6. Both samples exhibited the *A*2 ordering as identified by the (220) peak at 43°. No clear (200) peak was visible at 37.5° which again suggests the absence of *B*2 ordering.
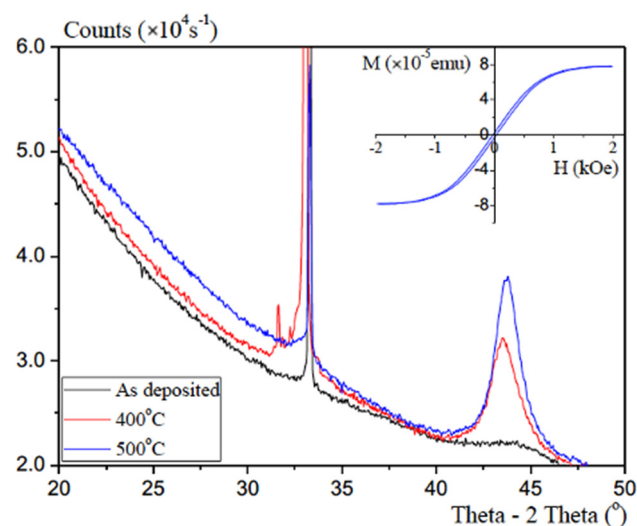

Figure 6. Representative XRD patterns of the Ni$_2$MnAl thin films doped with one Co peg as deposited and after two hours of annealing at 400 and 500 °C. The inset shows the corresponding magnetisation loop of the latter film. Note that the silicon substrate (200) peak and the fringes are visible at 33.2°.

As shown in Figure 7, the crystallisation also occurs at 300 °C, which is 150 °C lower than that for films without Co doping, which is favourable for device applications. The corresponding lattice constants were measured to be 0.8~2.9% larger than those for films without Co doping.

The crystallinity was also found to improve with increasing Co doping as shown in Figure 7. The magnetic response of the samples changed to ferromagnetic after post-annealing at 500 °C as shown in the inset of Figure 6, showing a magnetic moment of (76.2 ± 0.1) µemu, approximately 1.5 emu/cm^3, which is larger than that of the Fe substituted films. A possible cause for the ferromagnetism is the formation of Co$_2$MnAl grains because the films were annealed at the ordering temperature [15]. No further crystalline ordering was observed with increasing annealing and the corresponding magnetic properties were unchanged. This observation supports the hypothesis of the formation of Co$_2$MnAl as the cobalt content can be segregated from the Ni$_2$MnAl matrix, thus preventing further significant formation of grains. To eliminate such segregated grains, uniform compositional distributions within a film may be required, which is difficult to achieve using the doping method of the sputtering target used in this study. Even so, our study suggests a significant potential of Ni$_{2-x}$Co$_x$MnAl for robust antiferromagnetism at room temperature.
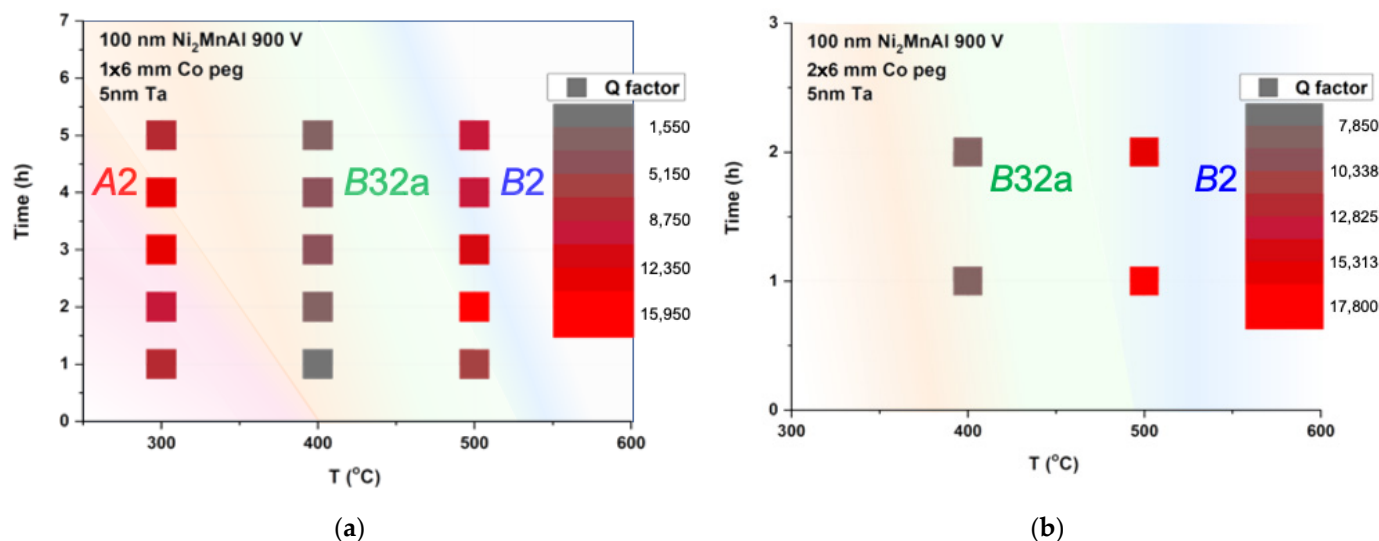
Figure 7. Crystallisation of the Ni_2MnAl thin films doped with (**a**) one and (**b**) 6 mm Co pegs indicated by Q factors.

4. Summary

We have grown and characterised a series of Ni_2MnAl Heusler alloy films. The films with one Co peg post-annealed at 500 °C for 2 h were found to show the highest crystalline ordering within the *A*2 phase but exhibited weak magnetic moments. For the demonstration of room-temperature antiferromagnetism, Fe and Co have been used to partially substitute for Ni. The Fe substitution showed an increase in the magnetic moment with increasing Fe content, which may be due to Fe segregation. On the other hand, Co substitution can effectively reduce the crystallisation temperature down to 300 °C but the corresponding magnetisation measurements proved that the *B*2-ordered $(Ni,Co)_2MnAl$ films showed ferromagnetic Co_2MnAl segregation as well. The segregated phases need to be eliminated by further compositional optimisation to achieve the stoichiometry while maintaining the reduced crystallisation in the pseudo-*B*2 phase temperature for antiferromagnetic spintronics.

References

1. Jungwirth, T.; Marti, X.; Wadley, P.; Wunderlich, J. Antiferroagnetic spintronics. *Nat. Nanotech.* **2016**, *11*, 231–241. [CrossRef] [PubMed]

2. Hirohata, A.; Huminiuc, T.; Sinclair, J.; Wu, H.; Samiepour, M.; Vallejo-Fernandez, G.; O'Grady, K.; Balluf, J.; Meinert, M.; Reiss, G.; et al. Development of antiferromagnetic Heusler alloys for the replacement of iridium as a critically raw material. *J. Phys. D Appl. Phys.* **2017**, *50*, 443001. [CrossRef]

3. Singh, S.; D'Souza, W.; Suard, E.; Chapon, L.; Senyshyn, A.; Petricek, V.; Skourski, Y.; Nicklas, M.; Felser, C.; Chadov, S. Room-temperature tetragonal non-collinear Heusler antiferromagnet Pt$_2$MnGa. *Nat. Commun.* **2016**, *7*, 1–6. [CrossRef] [PubMed]

4. Acet, M.; Duman, E.; Wassermann, E.F. Coexisting ferro- and antiferromagnetism in Ni$_2$MnAl Heusler alloys. *J. Appl. Phys.* **2002**, *92*, 3867–3871. [CrossRef]

5. Galanakis, I.; Şaşıoğlu, E. Structural-induced antiferromagnetism in Mn-based full Heusler alloys: The case of Ni$_2$MnAl. *Appl. Phys. Lett.* **2011**, *98*, 102514. [CrossRef]

6. Wu, H.; Vallejo-Fernandez, G.; Hirohata, A. Magnetic and structural properties of antiferromagnetic Mn$_2$VSi alloy films grown at elevated temperatures. *J. Phys. D Appl. Phys.* **2017**, *50*, 375001. [CrossRef]

7. Singh, D.J.; Mazin, I. Electronic structure, local moments, and transport in Fe$_2$VAl. *Phys. Rev. B* **1998**, *57*, 14352. [CrossRef]

8. Nayak, A.K.; Nicklas, M.; Chadov, S.; Khuntia, P.; Shekhar, C.; Kalache, A.; Baenitz, M.; Skourski, Y.; Guduru, V.K.; Puri, A.; et al. Design of compensated ferrimagnetic Heusler alloys for giant tunable exchange bias. *Nat. Mater.* **2015**, *14*, 679–684. [CrossRef] [PubMed]

9. Dong, X.Y.; Dong, J.W.; Xie, J.Q.; Shih, T.C.; McKernan, S.; Leighton, C.; Palmstrøm, C.J. Growth temperature controlled magnetism in molecular beam epitaxially grown Ni$_2$MnAl Heusler alloy. *J. Cryst. Growth* **2003**, *254*, 384–389. [CrossRef]

10. Tsuchiya, T.; Kubota, T.; Sugiyama, T.; Huminiuc, T.; Hirohata, A.; Takanashi, K. Exchange bias effects in Heusler alloy Ni$_2$MnAl/Fe bilayers. *J. Phys. D Appl. Phys.* **2016**, *49*, 235001. [CrossRef]

11. Huminiuc, T.; Whear, O.; Takahashi, T.; Kim, J.-Y.; Vick, A.; Vallejo-Fernandez, G.; O'Grady, K.; Hirohata, A. Growth and characterisation of ferromagnetic and antiferromagnetic Fe$_{2+x}$V$_y$Al Heusler alloy films. *J. Phys. D Appl. Phys.* **2018**, *51*, 325003. [CrossRef]

12. Elphick, K.; Frost, W.; Samiepour, M.; Kubota, T.; Takanashi, K.; Sukegawa, H.; Mitani, S.; Hirohata, A. Heusler alloys for spintronic devices: Review on recent development and future perspectives. *Sci. Technol. Adv. Mater.* **2021**, *22*, 235–271. [CrossRef] [PubMed]

13. Kanomata, T.; Kikuchi, M.; Yamauchi, H. Magnetic properties of Heusler alloys Ru$_2$MnZ (Z = Si, Ge, Sn and Sb). *J. Alloys Compd.* **2006**, *414*, 1–7. [CrossRef]

14. Ishida, S.; Kashiwagi, S.; Fujii, S.; Asano, S. Magnetic and half-metallic properties of new Heusler alloys Ru$_2$MnZ (Z = Si, Ge, Sn and Sb). *Phys. B* **1995**, *210*, 140–148. [CrossRef]

15. Sagar, J.; Fleet, L.R.; Walsh, M.; Lari, L.; Boyes, E.D.; Whear, O.; Huminiuc, T.; Vick, A.; Hirohata, A. Over 50% reduction in the formation energy of Co-based Heusler alloy films by two-dimensional crystallisation. *Appl. Phys. Lett.* **2014**, *105*, 032401. [CrossRef]